Ca^{2+}-Induced Movement of Tropomyosin in Skeletal Muscle Thin Filaments Observed by Multi-Site FRET

Corrado Bacchiocchi and Sherwin S. Lehrer
Muscle and Motility Group, Boston Biomedical Research Institute, Watertown, Massachusetts 02472 USA

ABSTRACT To obtain information on Ca^{2+}-induced tropomyosin (Tm) movement in Ca^{2+}-regulated muscle thin filaments, frequency-domain fluorescence energy transfer data were collected between 5-(2-iodoacetyl-amino-ethyl-amino)naphthalene-1-sulfonic acid at Cys-190 of Tm and phalloidin-tetramethylrhodamine B isothiocyanate bound to F-actin. Two models were used to fit the experimental data: an atomic coordinate (AC) model coupled with a search algorithm that varies the position and orientation of Tm on F-actin, and a double Gaussian distance distribution (DD) model. The AC model showed that little or no change in transfer efficiency is to be expected between different sites on F-actin and Tm if Ca^{2+} causes azimuthal movement of Tm of the magnitude suggested by structural data (C. Xu, R. Craig, L. Tobacman, R. Horowitz, and W. Lehman. 1999. *Biophys. J.* 77:985–992). However, Ca^{2+} produced a small but significant change in our phase/modulation versus frequency data, showing that changes in lifetime decay can be detected even when a change of the steady-state transfer efficiency is very small. A change in Tm azimuthal position of 17° on the actin filament obtained with the AC model indicates that solution data are in reasonable agreement with EM image reconstruction data. In addition, the data indicate that Tm also appears to rotate about its axis, resulting in a rolling motion over the F-actin surface. The DD model showed that the distance from one of the two chains of Tm to F-actin was mainly affected, further verifying that Ca^{2+} causes Tm to roll over the F-actin surface. The width of the distance distributions indicated that the position of Tm in absence and in presence of Ca^{2+} is well defined with appreciable local flexibility.

INTRODUCTION

Tropomyosin is an essential component of the F-actin·tropomyosin·troponin (F-actin·Tm·Tn) thin filament and provides the cooperativity for the regulation of muscle contraction (Lehrer and Geeves, 1998). Early x-ray structural studies on intact muscle fibers have suggested that Ca^{2+} binding to troponin (Tn) on striated muscle thin filaments caused a movement of tropomyosin (Tm) away from the myosin head binding site on F-actin, facilitating muscle contraction (Haselgrove, 1972; Huxley, 1972; Parry and Squire, 1973). Further evidence for a steric-blocking theory has been obtained with image reconstruction techniques on electron micrographs of F-actin·Tm·Tn thin filaments (Lehman et al., 1994; Xu et al., 1999). Yet solution evidence for this movement has been lacking. Early measurements of distance changes between specific labels on Tm and F-actin with fluorescence-detected resonance energy transfer (FRET) showed that, although significant energy transfer was obtained in the absence of Ca^{2+}, little or no change was observed due to the presence of Ca^{2+} (Miki et al., 1998; Tao et al., 1983). This indicated that either there was no movement or that the movement was such that the distance did not change because modeling indicated that, as the donor moved further from one acceptor it moved closer to another (Tao et al., 1983). More recent FRET studies with acceptor labels at different positions on F-actin and a donor at position 87 on Tm also showed no change in energy transfer due to the addition of Ca^{2+}, which was interpreted as no distance change between Tm and F-actin (Miki et al., 1998). The Tao et al. study was done by monitoring changes in lifetime using a photon-counting technique. The Miki et al. study utilized changes in fluorescence intensity monitored by steady-state techniques. We have reinvestigated this problem using a high-resolution, laser-excited, multi-frequency phase/modulation instrument together with global analyses of the donor-only and the donor–acceptor (D–A) decays to resolve lifetimes and distance distributions.

As in the previous study, the donor was 5-(2-iodoacetyl-amino-ethyl-amino)naphthalene-1-sulfonic acid (1,5-IAEDANS) at Cys-190 of rabbit skeletal $\alpha\alpha$ Tm but a different acceptor was used: phalloidin-tetramethylrhodamine B isothiocyanate conjugate (TRITC-Ph) at the phalloidin-binding site of F-actin. We obtained a small but significant Ca^{2+}-dependent difference in the phase/modulation data. Two different models were used to fit the data: an atomic coor-

Submitted August 22, 2001, and accepted for publication November 8, 2001.

Dr. Bacchiocchi's present address is Dipartimento di Chimica Fisica ed Inorganica, Università, Viale Risorgimento 4, 40136 Bologna, Italy. E-mail: Bacchio@bbri.org.

Address reprint requests to Sherwin S. Lehrer, Boston Biomedical Research Inst., Muscle & Motility Group, 64 Grove St., Watertown, Massachusetts 02472-2829. Tel.: 617-658-7812; Fax: 617-972-1753; E-mail: lehrer@bbri.org.

[1]The abbreviations used here are: Tm: tropomyosin; Tn: troponin; FRET: fluorescence-detected resonance energy transfer; S1: single-headed fragment of skeletal muscle myosin (myosin subfragment 1); 1,5-IAEDANS: 5-(2-iodoacetyl-amino-ethyl-amino)naphthalene-1-sulfonic acid; AEDANS: 1,5-IAEDANS after reaction with a sulfhydryl group; TRITC-Ph: phalloidin-tetramethylrhodamine B isothiocyanate conjugate; DABMI: 4-dimethylaminophenylazophenyl 4′-maleimide; DDPM: N-(4-dimethylamino-3,5-dinitrophenyl)maleimide; PPO: 2,5-diphenyloxazole; TNP-ADP: 2′ (or 3′)-O-(2,4,6-trinitrophenyl)-adenosine 5′-diphosphate; FLC: fluorescein cadaverine; FITC: fluorescein 5-isothiocyanate.

© 2002 by the Biophysical Society

0006-3495/02/03/1524/13 $2.00

dinate (AC) model, based on published atomic coordinates of F-actin·Tm (Lorenz et al., 1993, 1995) which varied the position and orientation of Tm on F-actin using fixed label positions on each chain of Tm and on each F-actin subunit; a double distance distribution (DD) model in which the "apparent" D–A distances (see next section) between each of the two donors on Tm and the array of acceptors on F-actin are fitted to two different distance distributions. Both models take into account the presence of two donors in different positions on Tm because each of the two Tm chains can be located at a different distance from the acceptor on the actin filament. The AC model showed that Ca^{2+} produced changes in Tm azimuthal position (around the F-actin axis) and axial orientation (around its own inter-chain axis) without appreciably affecting the transfer efficiency. The DD model showed that Ca^{2+} produced a large change in the distance of the label on one of the chains with only a small change in the distance of the label on the other chain to the actin filament. These results indicate that there is significant azimuthal movement of Tm with clear evidence for axial rotation associated with Ca^{2+}-binding to F-actin·Tm·Tn. A preliminary report of these results has been presented (Bacchiocchi and Lehrer, 2000).

THEORY

Multi-D–A atomic coordinate model

The theory of frequency-domain fluorometry can be applied to the study of energy transfer in a multi-donor, multi-acceptor-labeled protein complex in which the intensity decays (Lakowicz, 1999) are analyzed in terms of positions of the labeled proteins. The time-dependent fluorescence intensity decay is measured with a frequency-domain lifetime instrument that uses a sinusoidally modulated light source at different frequencies. At each light modulation frequency ω, the instrument measures the phase shift ϕ_ω and the demodulation m_ω of the fluorescence emission with respect to the excitation. For a given decay law $I(t)$, the phase ϕ_ω^c and the modulation m_ω^c can be calculated from the sine and cosine transforms N_ω and D_ω of $I(t)$:

$$\tan \phi_\omega^c = N_\omega/D_\omega, \tag{1}$$

$$m_\omega^c = (N_\omega^2 + D_\omega^2)^{1/2}, \tag{2}$$

where

$$N_\omega = \int_0^\infty I(t)\sin \omega t \, dt \Big/ \int_0^\infty I(t) \, dt, \tag{3}$$

$$D_\omega = \int_0^\infty I(t)\cos \omega t \, dt \Big/ \int_0^\infty I(t) \, dt. \tag{4}$$

We consider a D–A-labeled protein complex with only one donor and one acceptor species that can be found in multiple but spectroscopically equivalent positions (e.g., two donors in symmetric positions on the two chains of Tm and many acceptors, each one in an equivalent position, on the subunits of F-actin). In such a system, it is still possible to distinguish between different donor environments in terms of different arrangements of acceptors surrounding a given donor. The fluorescence intensity decay $I(t)$ of a D–A-labeled system of this kind can be expressed as a sum of exponential decays,

$$I(t) = \sum_n \alpha_n e^{-t/\tau_{da}^{(n)}}, \tag{5}$$

where $\tau_{da}^{(n)}$ is the lifetime of the donor in presence of acceptors in the nth environment and α_n is the fraction of donors in the nth environment. If the decay $I(t)$ is described by the sum of exponentials of Eq. 5, the transforms 3 and 4 can be derived analytically (Lakowicz et al., 1984),

$$N_\omega = \sum_n \frac{\alpha_n \omega \tau_{da}^{(n)^2}}{(1 + \omega^2 \tau_{da}^{(n)^2})} \Big/ \sum_n \alpha_n \tau_{da}^{(n)}, \tag{6}$$

$$D_\omega = \sum_n \frac{\alpha_n \omega \tau_{da}^{(n)}}{(1 + \omega^2 \tau_{da}^{(n)^2})} \Big/ \sum_n \alpha_n \tau_{da}^{(n)}. \tag{7}$$

α_n can be calculated from the structure and the symmetry of the system, $\tau_{da}^{(n)}$ is related to the donor lifetime in the absence of the acceptor τ_d and to the energy transfer rate $k_t^{(n)}$ in the nth environment by

$$\frac{1}{\tau_{da}^{(n)}} = \frac{1}{\tau_d} + k_t^{(n)}. \tag{8}$$

$k_t^{(n)}$ is, in turn, related to the D–A distances and to the critical transfer distance R_0 by

$$k_t^{(n)} = \frac{1}{\tau_d} \sum_i \left(\frac{R_0}{r_i^{(n)}}\right)^6, \tag{9}$$

where $r_i^{(n)}$ is the distance between one donor and the ith acceptor present in the nth environment.

In the rigid-body approximation, an appropriate AC model of the protein complex will provide the positions of the donors and acceptors, allowing the calculation of the distances $r_i^{(n)}$. The positions of the proteins are then varied to yield the best fit between the calculated phase shift ϕ_ω^c and the modulation m_ω^c and the corresponding experimental values ϕ_ω and m_ω, as indicated by a minimum value for the goodness-of-fit parameter χ_R^2,

$$\chi_R^2 = \frac{1}{\nu} \sum_\omega \left[\frac{\phi_\omega - \phi_\omega^c}{\delta\phi}\right]^2 + \frac{1}{\nu} \sum_\omega \left[\frac{m_\omega - m_\omega^c}{\delta m}\right]^2, \tag{10}$$

where ν is the number of experimental values of phase and modulation minus the number of variable parameters estimated

in the model, and $\delta\phi$ and δm are the uncertainties in the phase and modulation values, respectively.

Gaussian distance distribution model

The theory for energy transfer in the presence of a range of D–A distances has been presented and discussed in detail (Lakowicz et al., 1988) and subsequently extended (Cheung et al., 1991; Lakowicz et al., 1991) to take into account incomplete acceptor labeling. In case of a complete labeling and in the approximation of a static distance distribution within the fluorescence time scale, the intensity decay $I(t)$ is given by

$$I(t) = \sum_{j=1}^{M} \int_{x=0}^{\infty} F_j(x) \sum_{i=1}^{L} \alpha_{Di} \exp\left[-\frac{t}{\tau_{Di}} \left(1 + \left(\frac{R_0}{x} \right)^6 \right) \right] dx \tag{11}$$

where $F_j(x)$ is a suitable functional form for the distribution of the D–A distance x, and α_{Di} is the fractional amplitude of the ith donor relaxation τ_{Di}. The summations on i and j in Eq. 11 are extended to L exponential components of the donor decay and M different distance distributions, respectively. Assuming a Gaussian distance distribution model, we have

$$F_j(x) = a_j \frac{1}{\sigma_j (2\pi)^{1/2}} \exp\left[-\frac{1}{2} \left(\frac{x - r_j^c}{\sigma_j} \right)^2 \right], \tag{12}$$

where a_j is the fractional contribution of the jth distribution of mean distance r_j^c and width σ_j. The frequency response (phase shift ϕ_ω and demodulation m_ω) can be calculated by substituting the intensity decay law 11 in Eq. 3 and 4.

Apparent distance

According to Eq. 9, the D–A transfer rate k_t for a donor surrounded by N acceptors is

$$k_t = \frac{1}{\tau_d} \sum_{i=1}^{N} \left(\frac{R_0}{r_i} \right)^6. \tag{13}$$

The above relation holds because the energy transfer rates are additive, and a set of acceptors (e.g., the array of acceptors on F-actin) surrounding a given donor will behave as a single deactivation channel of the donor excitation energy or, in other words, as an "apparent" single acceptor. The corresponding apparent distance r_a can be defined as the D–A separation such that

$$k_t = \frac{1}{\tau_d} \left(\frac{R_0}{r_a} \right)^6. \tag{14}$$

From Eq. 13 and 14, after simple algebra we have

$$r_a = \left(\sum_{i=1}^{N} \frac{1}{r_i^6} \right)^{-1/6}. \tag{15}$$

This distance is particularly interesting for us, because it represents the D–A distance "seen" by a FRET experiment.

EXPERIMENTAL PROCEDURES

Materials

1,5-IAEDANS was from Molecular Probes (Eugene, OR), TRITC-Ph was from Fluka, 2,5-diphenyloxazole (PPO) was from Sigma. Other materials used for buffers, solutions, and routine analysis were from Sigma.

Protein preparation

Preparation of rabbit skeletal $\alpha\alpha$ Tm, F-actin, Tn as well as the 1,5-IAEDANS labeling of Tm, the determination of the fraction of F-actin-bound Tm, and labeling ratio of Tm were described elsewhere (Lamkin et al., 1983). TRITC-Ph-labeled F-actin was prepared by incubating F-actin (22 μM) with 1 equivalent of TRITC-Ph (added from a 1 mg/ml methanol stock solution) in F-buffer (10 mM Hepes, 50 mM NaCl, 5 mM $MgCl_2$ and 0.1 mM $CaCl_2$, pH 7.5) at 4°C for 24 h to allow complete saturation of binding sites. The final volume of methanol was always below 3%. The labeling ratio of actin was determined by centrifuging the TRITC-Ph-labeled F-actin sample at 85,000 $\times$ g for 60 min, followed by resuspension of the pellet in F-buffer and measurement of the TRITC-Ph absorbance at 552 nm ($\epsilon_{552}^{\text{TRITC-Ph}} = 85 \times 10^3\ M^{-1}\,cm^{-1}$ (Waggoner et al., 1989)). Typical labeling ratios were 0.55–0.65 for Tm and 0.80–0.85 for F-actin. A typical sample composition was [Tm] = 2.0 μM; [F-actin] = 20.0 μM; [Tn] = 3.0 μM; [Ca^{2+}] = 0.1 mM, or [EGTA] = 1.0 mM in F-buffer, pH 7.5 at 25°C. We used an excess of F-actin and Tn to limit the presence of donor-labeled Tm not bound to F-actin, thus minimizing the amount of donor fluorescence not quenched by the acceptor. In practice, a certain amount of unquenched donor fluorescence is always present in this kind of experiment and, even if we can take it into account in the analysis (see the Results section), it must be kept as low as possible because it does not provide any information about D–A distances, thereby reducing the quality of the FRET measurements. Using an excess of F-actin and Tn does not introduce other unwanted fluorescence signals because Tn is not labeled and the TRITC-Ph emission is accurately filtered out (see next section).

Fluorescence lifetime measurements

Frequency-domain fluorescence data were collected at 25°C with an ISS K2 Cross-Correlation, Phase and Modulation Fluorometer (ISS Co., Urbana, IL), using the 325-nm excitation of a Liconix 4042NB He-Cd laser. Twenty-five frequencies were recorded between 2 and 200 MHz for each measurement. A 500-nm interference filter, 30-nm bandwidth was used to isolate the AEDANS (1,5-IAEDANS after reaction with a sulfhydryl group) emission and to reject excitation light and the emission of the acceptor, TRITC-Ph. A 20-μM PPO solution in ethanol was used as reference (1.4 ns mono-exponential decay (Lakowicz, 1999)). A pair of

identical 4-mm light-path cuvettes was used in all measurements to avoid inner filter effects and to minimize the targeting error (Lakowicz, 1999). The acquisition statistics of the instrument was set to a standard deviation $\delta\phi = 0.2°$ for the phase and $\delta m = 0.005$ for the modulation.

ATPase activity assays

We tested each FRET system for ATPase activity to ensure that labeled proteins were not altered in binding or function. The Enzchek colorimetric phosphate assay (Molecular Probes) showed similar levels of actin-myosin single-headed fragment of skeletal muscle myosin subfragment 1 (S1)-activated ATPase activity and similar Tm inhibition for AEDANS-labeled and unlabeled Tm. Tn samples conferred Ca^{2+} sensitivity to the ATPase of labeled and unlabeled systems. TRITC-Ph did not affect the ATPase activity of F-actin·S1. Absorption measurements were made in a DU650 Beckman spectrophotometer. Steady-state fluorescence measurements were conducted in a LS50B Perkin Elmer fluorometer.

COMPUTATIONAL DETAILS

Critical transfer distance R_0

The critical transfer distance R_0 (Å) was calculated according to Förster (1948) by using (Van Der Meer et al., 1991)

$$R_0 = 0.211(Q\kappa^2 n^{-4} J)^{1/6}, \tag{16}$$

where Q is the donor quantum yield, κ^2 is an orientation factor, n is the refractive index of the medium, and J ($cm^{-1}\,M^{-1}\,nm^4$), defined as

$$J = \int F(\lambda)\epsilon(\lambda)\lambda^4\,d\lambda \Big/ \int F(\lambda)\,d\lambda, \tag{17}$$

is the overlap integral between the fluorescence intensity $F(\lambda)$ of the donor and the molar extinction coefficient $\epsilon(\lambda)$ of the acceptor.

The critical transfer distance R_0 (Å) for the AEDANS-TRITC-Ph D–A pair was calculated using the following values. The quantum yield of AEDANS-labeled Tm and F-actin·Tm was taken to be 0.53 (Van Der Meer et al., 1991; Tao et al., 1983). When complexed with Tn, the AEDANS-labeled Tm quantum yield increased by a factor of 1.2 irrespective of Ca^{2+} concentration. The refractive index of the medium was taken to be 1.4 (Van Der Meer et al., 1991) and the orientation factor κ^2 was assumed to be ⅔ (see Discussion). The overlap integral J was calculated by numerical integration at 1-nm intervals using Simpson's rule and was found to be $2.44 \times 10^{15}\ cm^{-1}\,M^{-1}\,nm^4$. From these values we obtained $R_0 = 52.0$ Å for F-actin·Tm and $R_0 = 53.5$ Å for F-actin·Tm·Tn.

Atomic coordinate model

An AC model (Lorenz et al., 1993, 1995) (see Fig. 1) was used to fit the frequency response (phase and modulation data) of AEDANS donor-labeled Tm and TRITC-Ph acceptor-labeled F-actin in the F-actin·Tm and F-actin·Tm·Tn

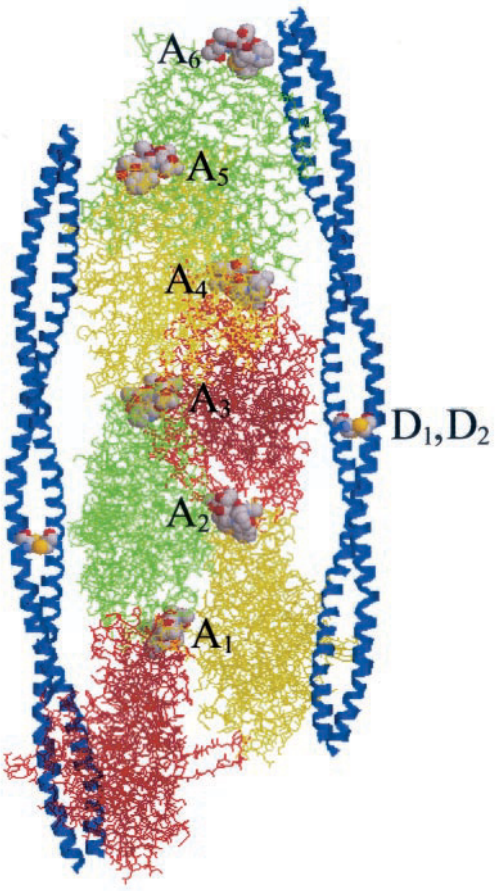

FIGURE 1 Atomic coordinate model of the F-actin·Tm complex from Lorenz et al. (1993, 1995). The model is formed by six actin monomers (*wire-frame*) and 2 Tm molecules (*blue ribbons*) on opposing sides of the F-actin helix. The donor and acceptor sites (*space-fill*) are Cys-190 on Tm (D_1 and D_2) and the phalloidin binding site on each actin monomer (A_1–A_6). Displayed using the program Rasmol (Bernstein, 1999).

($\pm Ca^{2+}$) complex, using the equations presented above. The AC model used the coordinates of F-actin with ADP, metal and phalloidin (Lorenz et al., 1993), and the coordinates of Tm bound to actin, model-built as described (Lorenz et al., 1995). Mean label positions were modeled as rigid segments attached to the sulfur atoms of the two Cys-190 of Tm, or to the β carbon of the hydroxyleucine of phalloidin on F-actin. Details about the chosen D–A positions are presented in the Discussion section.

Model parameters were calculated as follows. The fraction, α_n, of donors in the nth donor environment (see Eq. 5, 6, and 7) is related to the fraction of F-actin-bound Tm, f_b, and the fraction of acceptor labeling, f_l. In particular, the donors attached to the unbound Tm do not see any acceptors, therefore $\alpha_n = 1 - f_b$. Given the different combinations of actin acceptors surrounding the donors on the bound Tm, we can calculate the fraction of donors in each environment as follows. We start by defining an appropriate size of the environment, to take into account all the significant

TABLE 1 Three exponential decay parameters for donor-labeled Tm alone and in complex with F-actin and Tn ($\pm Ca^{2+}$)

Sample	τ_{D1} (ns)	α_{D1}	τ_{D2} (ns)	α_{D2}	τ_{D3} (ns)	α_{D3}	χ^2_R
Tm	13.3 ± 0.1	0.73 ± 0.07	3.3 ± 0.5	0.14 ± 0.02	0.5 ± 0.3	0.13 ± 0.06	1.3
F-actin·Tm	14.0 ± 0.3	0.65 ± 0.05	7 ± 1	0.19 ± 0.04	1.1 ± 0.1	0.16 ± 0.01	1.0
F-actin·Tm·Tn ($-Ca^{2+}$)	15.4 ± 0.3	0.65 ± 0.05	7 ± 1	0.14 ± 0.03	1.37 ± 0.08	0.21 ± 0.01	1.0
F-actin·Tm·Tn ($+Ca^{2+}$)	15.8 ± 0.7	0.59 ± 0.08	9 ± 2	0.2 ± 0.1	1.5 ± 0.1	0.22 ± 0.01	1.5

D–A interactions while keeping the computing time to a reasonable amount. Our choice was to consider only the individual transfers with an efficiency larger than 5%, which corresponds, for $R_0 = 53.5$ Å, to a D–A distance cutoff radius of ≈90 Å and, in practice, it means to consider six actin subunits closest to the donors (see Fig. 1). Having two possibilities for an acceptor on each actin subunit (present or not), there are $2^6 = 64$ possible different arrangements of acceptors around the donors. The fraction, α_n, of donors in each one of these environments is given by

$$\alpha_n = \tfrac{1}{2} f_b f_l^p (1 - f_l)^{1-p}, \tag{18}$$

with $p = \sum_{i=1}^{6} P_i$, where P_i is equal to one or zero according to whether the acceptor is present or absent in the ith subunit, respectively. The D–A lifetime $\tau_{da}^{(n)}$, corresponding to the nth environment, is calculated using Eq. 8 and 9, where the D–A distances $r_i^{(n)}$ are given by the AC model. The steady-state transfer efficiency E^c can be calculated as (Lakowicz, 1999)

$$E^c = \frac{\sum_n \alpha_n \tau_{da}^{(n)}}{\tau_d}. \tag{19}$$

Experimental data were fitted using a search algorithm that inputs the Tm and F-actin atomic coordinates and systematically varies the Tm position on F-actin (both proteins are considered as rigid bodies) by changing the azimuthal position (angle around the F-actin axis), the axial orientation (angle around Tm own inter-chain axis) and the radial position (distance between the Tm axis and the F-actin axis). Angles are calculated with respect to the original (unchanged) Lorenz position. A positive angle represents a clockwise Tm rotation as viewed from the F-actin pointed end. The parameters representing the fraction of bound Tm f_b^c and the F-actin labeling ratio f_l^c were also systematically varied. Each combination of parameters is used as initial guess for the fit, which is performed with an implementation of the Minpack Fortran libraries (Moré et al., 1980), which uses a modified version of the least-squares Levenberg–Marquardt algorithm. Confidence intervals were estimated at a probability of 95% using a Monte-Carlo method (Straume and Johnson, 1992).

Distance distribution model

To obtain information about the flexibility of the D–A-labeled F-actin·Tm and F-actin·Tm·Tn ($\pm Ca^{2+}$) complex, the frequency-domain phase and modulation data were also analyzed in terms of the Gaussian distance-distribution model described above (Eq. 11). In this model, the protein complex is assumed to be rigid on the energy-transfer time scale but flexible on a longer time scale, resulting in a static distribution of D–A distances. According to our previous discussion, the distances between each donor on Tm and the acceptors on F-actin can be combined in an apparent distance (Eq. 15). In particular, having two donors on Tm, there will be two different apparent distances to be recovered by the fit but with the same distribution width σ, due to the symmetry of the Tm molecule.

Data were fitted using the GAUDIS fitting function (CFS–LS global fitting program (Johnson, 2000)), which implements the Gaussian distance distribution model of Eq. 11 and can also fit the fraction of acceptor labeling f_l (Cheung et al., 1991; Lakowicz et al., 1991). Before fitting experimental data, we tested against simulated data sets, the capability of the GAUDIS model to resolve the required two distance distributions. By using the AC model described above, we simulated frequency-domain phase and modulation data due to energy transfer from each one of the two donors on Tm to the acceptors on the F-actin subunits. Values of the parameters used in the simulations were comparable to those found for the F-actin·Tm·Tn complex and are presented in the Results section.

RESULTS

Donor-only fluorescence decays

The phase and modulation data of the donor-only samples were fitted to one, two, and three exponentials (CFS–LS global fitting program, HETANL1, 2, and 3 fitting functions (Johnson, 2000)). Even though the decay was only slightly heterogeneous (see Table 1 and Fig. 2), a one- or two-exponential model gave values of χ^2_R larger than 100 or 10, respectively. A large change in the two shorter lived components occurred when Tm formed a complex with F-actin (Table 1). Because both these components have a small fractional contribution to the total decay, α_{D2} and α_{D3}, the phase and modulation data for Tm and F-actin·Tm are very similar (Fig. 2 *a*). The complex with Tn also introduced a change in the main component, probably due to a decrease in the local polarity. The resulting decays, which are almost independent of $[Ca^{2+}]$, differ somewhat from F-actin·Tm

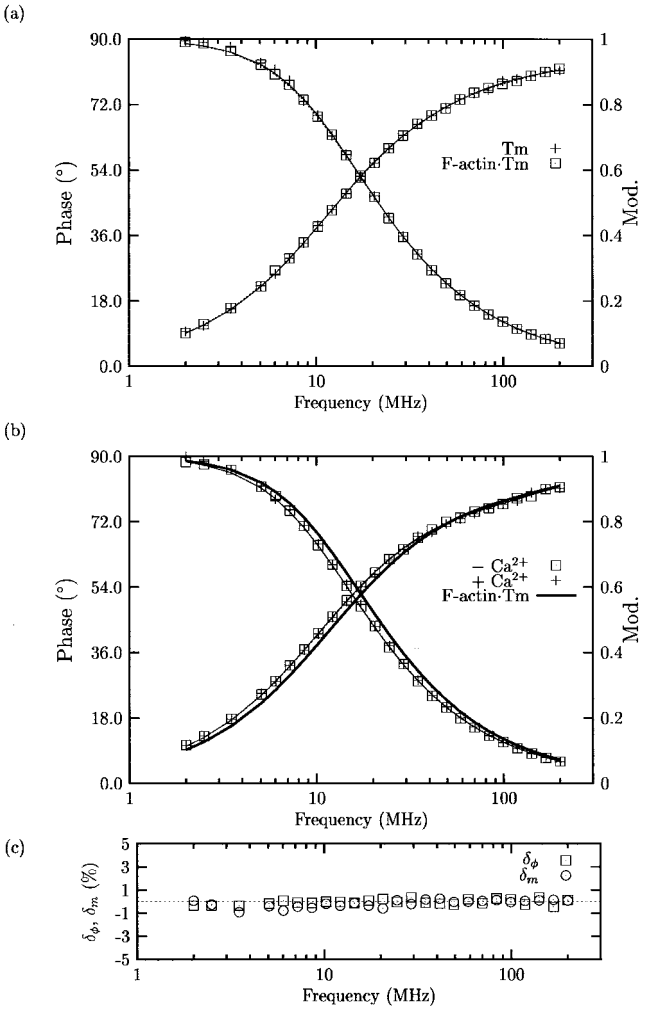

FIGURE 2 Frequency-domain phase and modulation data and fits for donor-labeled Tm alone and in complex with F-actin and Tn. The parameters recovered from the fit are reported in Table 1. The phase angle increases and the modulation decreases with increasing frequency. (*a*) Tm (+), F-actin·Tm (□); (*b*) F-actin·Tm·Tn in absence (□) and in presence (+) of Ca^{2+}. The F-actin·Tm fit (*thicker line*) is shown for comparison. (*c*) Phase (δ_ϕ) and modulation (δ_m) residuals for a typical fit.

(Fig. 2 *b*). The residuals of the fit had small and random deviations (Fig. 2 *c*).

Steady-state energy transfer data are not sensitive to Ca^{2+}-induced movement

We explored the possibility of reproducing published steady-state energy-transfer data by using the AC model, described above. This application can be considered also as a test for the model itself. We chose the work of Miki et al. (1998), who studied the energy transfer efficiency E between AEDANS (donor) attached to the unique Cys residue in position 87 of a mutant (Ser87Cys/Cys190Ser) $\alpha\alpha$Tm and different probes (acceptor) attached to various F-actin sites in the reconstituted thin filament in the absence and presence of Ca^{2+}. The results are presented in Table 2. The $+Ca^{2+}$ state was modeled using the Tm position obtained by minimizing the electrostatic energy of the F-actin–Tm interaction (Lorenz et al., 1995). An azimuthal rotation of $-25°$ of Tm, taken with respect to the Lorenz position, was used to model the $-Ca^{2+}$ state. Donor positions on Tm were modeled as described above using the β carbon on Ser-87 of the Tm model as an attachment site for the label. Acceptor positions on F-actin are modeled using the α-carbon coordinates of the labeled residue. We can see that there is good agreement between calculated and experimental values (Table 2). In particular, the model clearly predicts that only a small difference in transfer efficiency is expected when Tm moves azimuthally. In all cases, the calculated energy-transfer efficiency E^c differs by less than 0.05 between the $\pm Ca^{2+}$ modeled states. This difference is comparable or even smaller than the error normally present in a fluorescence steady-state measurement.

TABLE 2 Effect of $[Ca^{2+}]$ on experimental energy transfer efficiency values *E* between donor-labeled Tm and acceptor-labeled F-actin, compared to values calculated with the atomic coordinate model (E^c, see text)

F-actin Labeling Site	Acceptor	f_1	R_0 (Å)	$-Ca^{2+}$ E	$-Ca^{2+}$ E^c	$+Ca^{2+}$ E	$+Ca^{2+}$ E^c
Nucleotide	TNP-ATP	0.67	41.4	0.49	0.45	0.49	0.46
Gln-41	FLC	0.71	47.2	0.45	0.45	0.45	0.42
Lys-61	FITC	1.0	47.1	0.49	0.49	0.42	0.48
Cys-374	DABMI	1.0	40.0	0.32	0.33	0.32	0.31

The donor was AEDANS attached to Cys-87 (Miki et al., 1998). f_1, Fraction of acceptor-labeled F-actin; TNP-ADP, 2′ (or 3′)-O-(2,4,6-trinitrophenyl)-adenosine 5′-diphosphate; FLC, fluorescein cadaverine; FITC, fluorescein 5-isothiocyanate; DAB-MI, 4-dimethylaminophenylazophenyl 4′-maleimide.

Atomic coordinate model fits of experimental data

The phase and modulation data for the AEDANS-TRITC-Ph D–A-labeled F-actin·Tm·Tn complex showed small but clear differences due to binding of Ca^{2+} to Tn (Fig. 3 *a*). We also obtained phase and modulation data for the same donor-labeled protein complex using 4-dimethylaminophenylazophenyl 4′-maleimide (DABMI) as acceptor on F-actin's Cys-374. Using TRITC-Ph as acceptor, we were able to obtain greater sensitivity to Ca^{2+} (Fig. 3 *b*). The F-actin·Tm·Tn ($-Ca^{2+}$) data were fitted with a search centered on a Tm azimuthal position of $-25°$ and a radial position corresponding to the Lorenz coordinates, searching over a range of $\pm 30°$ and ± 2 Å, respectively, optimizing the search parameters and the Tm axial orientation at each step. The fit of the F-actin·Tm·Tn ($+Ca^{2+}$) complex data was obtained in the same way with a search centered on a Tm position corresponding to the original Lorenz coordi-

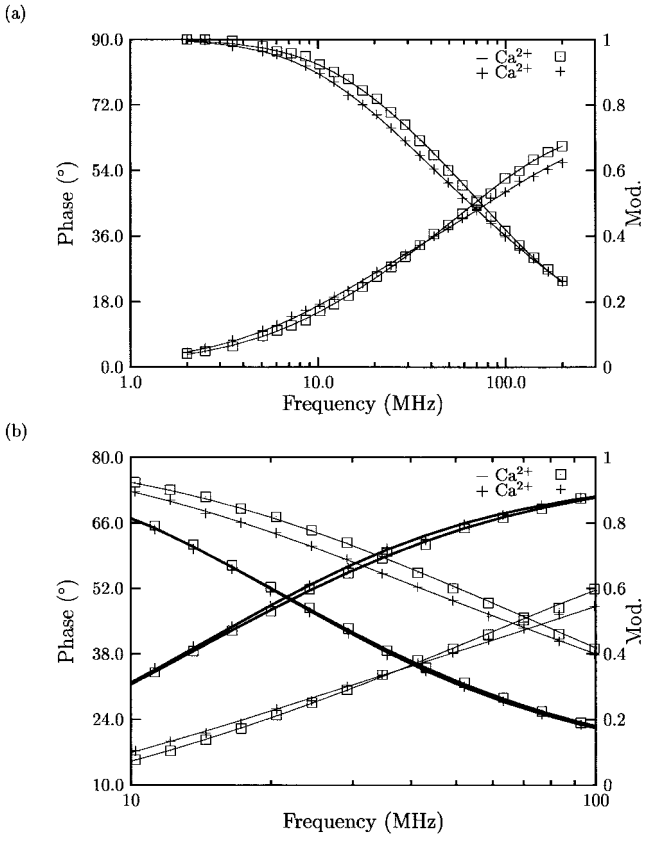

FIGURE 3 (*a*) Frequency-domain phase and modulation data in presence of energy transfer and fits for AEDANS donor- and TRITC-Ph acceptor-labeled F-actin·Tm·Tn complex in absence (□) and in presence (+) of Ca^{2+}. The fits were done using the thin filament atomic coordinate model (see text). The parameters recovered from the fits are reported in Table 3. (*b*) Detail of the fit in (*a*) (*thinner line*); experimental data and fit for the AEDANS donor and DABMI acceptor-labeled F-actin·Tm·Tn complex in absence (□) and in presence (+) of Ca^{2+} (*thicker line*).

nates. The fraction of bound Tm f_b^c and the F-actin labeling ratio f_1^c were also systematically varied, before each optimization cycle, around the measured values of 0.98 ± 0.02 and 0.85 ± 0.03, respectively, with a range of variation of 0.9–1.0 and 0.75–0.9, respectively.

We obtained an acceptable fit of the F-actin·Tm·Tn ($-Ca^{2+}$) data with some uncertainty of the Tm azimuthal position and axial orientation (Table 3). The fit of the F-actin·Tm·Tn ($+Ca^{2+}$) data is less good and therefore shows a larger uncertainty of the Tm position. The fitted transfer efficiency, E^c, was 0.86 for both data, in good agreement with the experimental value of 0.83 ($-Ca^{2+}$) and 0.85 ($+Ca^{2+}$). The Tm positions corresponding to the parameters reported in Table 3 are shown in Fig. 4. At low [Ca^{2+}], Tm is between the outer and the inner domain of F-actin, partially covering sites on F-actin required for myosin binding (Rayment et al., 1993). At high [Ca^{2+}], Tm moves ≈17° azimuthally and 46° axially, with little radial position change, uncovering the strong myosin binding

TABLE 3 Atomic coordinate model fit of the frequency-domain phase and modulation data of the AEDANS donor- and TRITC-Ph acceptor-labeled F-actin·Tm·Tn complex in absence and in presence of Ca^{2+}

Parameters	$-Ca^{2+}$	$+Ca^{2+}$
χ^2_R	1.6	2.9
Tm azimuthal position	−14 ± 12°	3 ± 13°
Tm radial position	39 ± 1 Å	40 ± 1 Å
Tm axial orientation	113 ± 35°	159 ± 46°
Fraction of bound Tm	0.99	0.97
Actin labeling ratio	0.80	0.82
Transfer efficiency E^c	0.86	0.86

sites. The azimuthal shift is in good agreement with structural studies (Xu et al., 1999).

Distance distribution model fits of simulated data

To determine if a double DD model would be appropriate to fit our data, we used the thin filament AC model described

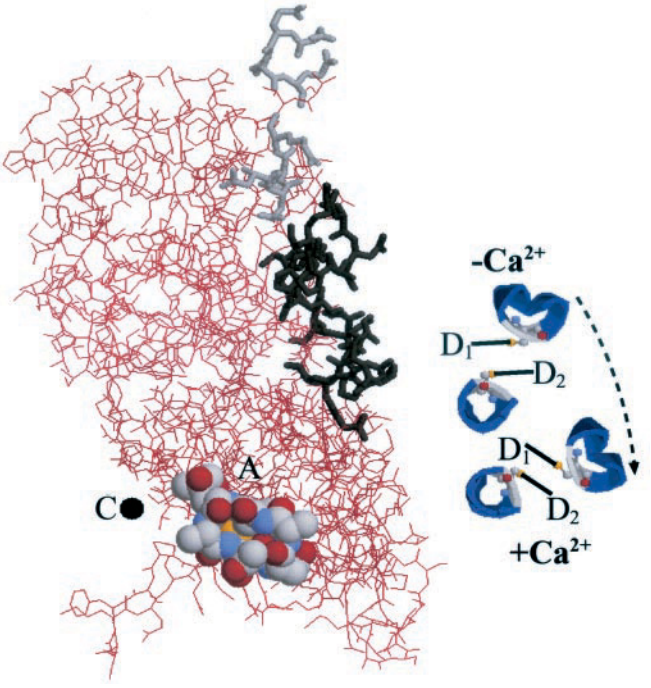

FIGURE 4 Ca^{2+}-induced movement of Tm obtained from the atomic coordinate model (see text). The longitudinal view of the thin filament along the F-actin axis (*C*) shows only one actin monomer (*red wire-frame*) and the Tm region around the donor position at Cys-190 (Glu-187 to Leu-193, *blue ribbons*). The thicker portion of the wire-frame rendering located on the surface of F-actin indicates the residues reported to interact with myosin (Rayment et al., 1993). Actin residues 1–4 and 92–95 (*grey*): weak myosin-binding; residues 24–28, 340–346, 144–148, and 332–336 (*black*): strong myosin-binding. The donor and acceptor sites are Cys-190 on Tm (D_1 and D_2) and the phalloidin binding site on the actin monomer (A). The blue ribbon rendering shows the fitted Tm positions in absence and in presence of Ca^{2+}. The fitted Tm movement is mainly a combination of an azimuthal (around the F-actin axis) and an axial (around its own inter-chain axis) rotation (see Table 3). Displayed using the program Rasmol (Bernstein, 1999).

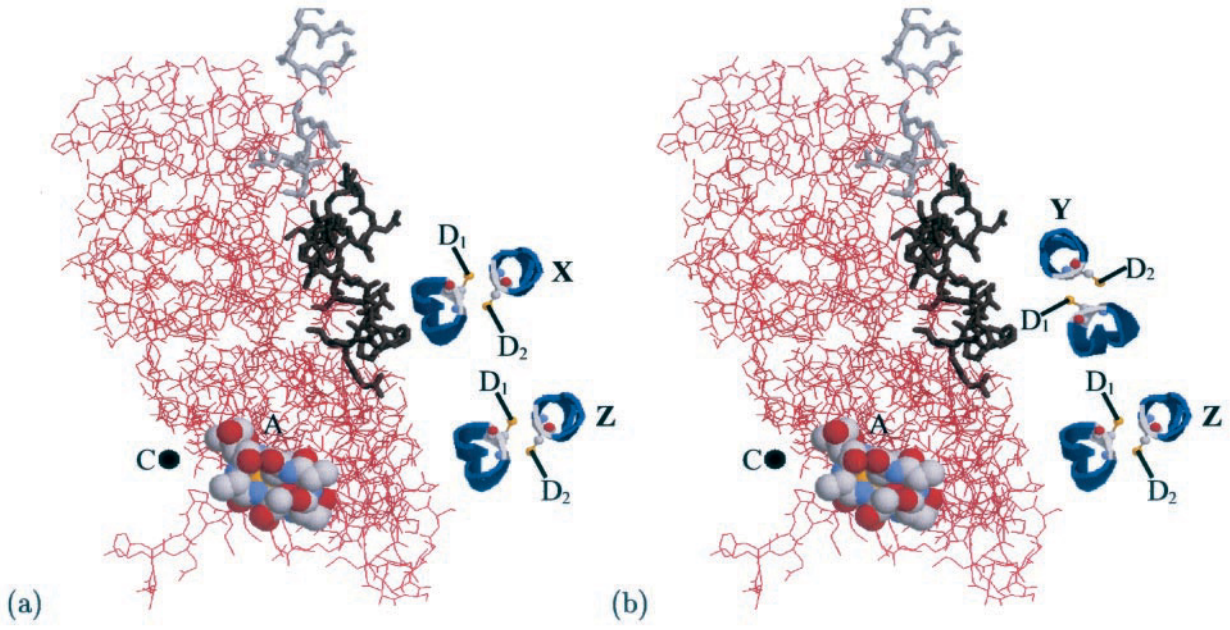

FIGURE 5 Tm positions (*X*, *Y*, *Z*) adopted to simulate data sets used to test the distance distribution model (see Table 5). The rendering of the thin filament longitudinal view is the same as in Fig. 4. The Tm positions adopted were obtained by changing the Tm azimuthal position (around the F-actin axis) and axial orientation (around its own inter-chain axis) with respect to the model for the F-actin·Tm complex proposed by Lorenz et al. (1993, 1995). The $-Ca^{2+}$ state was modeled in two different ways, assuming either a Tm azimuthal rotation of $-25.0°$ (*X*), or an azimuthal rotation of $-25.0°$ plus an axial rotation of $-90.0°$ (*Y*). The $+Ca^{2+}$ state (*Z*) was modeled using the unchanged Lorenz Tm position. Displayed using the program Rasmol (Bernstein, 1999).

above to simulate sets of data of the frequency response (phase and modulation) due to energy transfer between AEDANS on Tm Cys-190 and TRITC-Ph on F-actin. The simulated data were then analyzed in terms of the DD model to obtain best fits to two distances r_1^c and r_2^c with the same distribution width σ. These distances were then compared with apparent distances r_{a1} and r_{a2} calculated from the AC model using Eq. 15. The data sets were simulated using a different combination of the fraction of acceptor-labeled F-actin f_l, the fraction of F-actin-bound Tm f_b and the Tm position on F-actin (to model the $\pm Ca^{2+}$ states). The parameters used to simulate the data sets were as follows: data set 1: $f_l = 1.0, f_b = 1.0$; data set 2: $f_l = 1.0, f_b = 0.9$; data set 3: $f_l = 0.8, f_b = 1.0$; data set 4: $f_l = 0.8, f_b = 0.9$. The Tm positions adopted were obtained by changing the Tm azimuthal position and axial orientation with respect to the F-actin·Tm model proposed by Lorenz et al. (1995) and are shown in Fig. 5. The $-Ca^{2+}$ state was modeled in two different ways, assuming either a Tm azimuthal rotation of $-25.0°$ (Fig. 5 *a*, *X*), or an azimuthal rotation of $-25.0°$ plus an axial rotation of $-90.0°$ (Fig. 5 *b*, *Y*). The $+Ca^{2+}$ state (Fig. 5, *Z*) was modeled using the unchanged Lorenz Tm position. The distances between each of the two donors (Fig. 1, D_1 and D_2) on Cys-190 of Tm and the six closest acceptors (Fig. 1, A_1–A_6) at the phalloidin binding site of F-actin, for the modeled Tm positions *X*, *Y*, and *Z*, are listed in Table 4. The tri-exponential donor-only decay was modeled using the following values: $\tau_{D1} = 15.5$ ns, $\alpha_{D1} = 0.65$, $\tau_{D2} = 7.3$ ns, $\alpha_{D2} = 0.14$, $\tau_{D3} = 1.4$ ns, $\alpha_{D3} = 0.21$. A Gaussian-distributed error with standard deviation $\delta\phi$ of $0.2°$ for the phase and δm of 0.005 for the modulation was added to the simulated data sets. The data were analyzed using the CFS–LS global fitting program (Johnson, 2000)

TABLE 4 D–A distances (Å) from the two donors (AEDANS), D_1 and D_2, at Cys-190 of Tm, to each of six neighbor acceptor (TRITC-Ph), A_1–A_6 (Fig. 1), on the F-actin subunits, calculated according to Lorenz model (Lorenz et al., 1993, 1995), for the Tm azimuthal positions (around the F-actin axis) and axial orientations (around its own inter-chain axis) shown in Fig. 5

	A_1	A_2	A_3	A_4	A_5	A_6
Tm position *X*						
D_1	65.75	**37.49**	45.55	39.70	75.63	89.32
D_2	77.37	42.70	54.90	**39.62**	76.49	87.25
Tm position *Y*						
D_1	64.56	**30.75**	42.00	35.78	72.43	88.52
D_2	79.98	49.62	60.09	**44.96**	81.40	88.90
Tm position *Z*						
D_1	65.89	**31.16**	43.75	36.54	73.22	89.04
D_2	81.07	44.24	58.50	**43.57**	77.85	90.18

Details about the modeling of the location of the donors and the acceptors in the protein structures are presented in the Discussion section. For each donor, the shortest D–A distance is shown in boldface.

TABLE 5 Double Gaussian distance distribution analysis of simulated data

Data Set	f_l	f_b	f_l^c ($\equiv f_b^c$)	r_1^c (Å)	r_2^c (Å)	σ (Å)	χ^2_R
Tm position *X* r_{a1} = 33.2 Å r_{a2} = 35.8 Å							
1	1.0	1.0	1.0*	33.1 ± 0.2	35.8 ± 0.1	0.0	1.04
2	1.0	0.9	0.90 ± 0.01	33.2 ± 0.4	35.8 ± 0.2	0.0	1.04
3	0.8	1.0	0.99 ± 0.01	34.4 ± 0.6	37.4 ± 0.4	3.4	1.34
4	0.8	0.9	0.89 ± 0.01	34.8 ± 0.8	37.1 ± 0.4	3.4	1.35
Tm position *Y* r_{a1} = 28.5 Å r_{a2} = 40.8 Å							
1	1.0	1.0	1.0*	28.4 ± 0.4	40.8 ± 0.1	0.0	1.01
2	1.0	0.9	0.90 ± 0.01	29 ± 1.2	41.0 ± 0.4	0.0	1.06
3	0.8	1.0	0.99 ± 0.01	29.6 ± 0.8	42.6 ± 0.2	3.4	1.29
4	0.8	0.9	0.90 ± 0.01	29 ± 1.6	42.5 ± 0.4	3.4	1.39
Tm position *Z* r_{a1} = 29.0 Å r_{a2} = 38.4 Å							
1	1.0	1.0	1.0*	29.1 ± 0.8	38.3 ± 0.1	0.0	1.10
2	1.0	0.9	0.90 ± 0.01	29.6 ± 0.8	38.4 ± 0.1	0.0	1.09
3	0.8	1.0	0.99 ± 0.01	30.3 ± 0.4	40.3 ± 0.1	3.4	1.25
4	0.8	0.9	0.89 ± 0.01	30.4 ± 0.6	40.3 ± 0.1	3.4	1.36

*Was kept fixed in the fit.

Tm positions *X*, *Y*, and *Z* were modeled as described in the text and are shown in Fig. 5; details of the simulation are in the text.

f_l, f_b, fraction of acceptor labeling and fraction of F-actin-bound Tm used to simulate the data set, respectively; r_{a1}, r_{a2}, values of the apparent D–A distances calculated with Eq. 15 using, for each modeled Tm position, the distances listed in Table 4.

Parameters recovered from the fits are: r_1^c, r_2^c, D–A distances; f_l^c, fraction of acceptor labeling (the equivalence between f_l^c and f_b^c for this particular D–A system is discussed in the text); σ, width of the distance distribution.

(GAUDIS fitting function). Recovered D–A distances r_1^c and r_2^c and other parameters are listed in Table 5. All fits were performed by fixing σ to the same value for both distances, due to the symmetry of the Tm molecule, optimizing the fraction of acceptor labeling f_l^c and the D–A distances r_1^c and r_2^c and then repeating the optimization for a different value of σ until the best possible fit was achieved. The goodness of the fits was assessed by the χ^2_R values (Table 5, last column) and by the analysis of the residuals (not shown). All confidence intervals were calculated at a probability of 95% and were obtained with the Support-Plane method (Johnson, 2000).

In all fits listed in Table 5, the recovered distances r_1^c and r_2^c are in very good agreement with the corresponding apparent distances r_{a1} and r_{a2} calculated with Eq. 15 using the D–A distances listed in Table 4 and assuming complete acceptor labeling. In the case of partial labeling or in the presence of unbound Tm (data sets 2–4), the agreement between the recovered and the apparent distances is still good, with differences smaller than 2 Å. From the goodness of the fits and from this result, we conclude that the double-distance distribution model is capable to recover two apparent D–A distances with acceptable uncertainties even in the presence of unbound Tm and of incomplete acceptor labeling, which, as we discuss next, introduces an "apparent distance distribution" in the results.

The width of the distance distribution σ is reported in the penultimate column of Table 5. For data sets 1 and 2, the recovered σ is, as expected, zero, because the AC model, used to simulate the data sets, was assumed to be rigid. However, a σ of 3.4 Å was obtained in the analysis of data sets 3 and 4, where the fraction of acceptor labeling f_l is 0.8. This occurs because not all the F-actin subunits are labeled and therefore different arrangements of acceptors, surrounding a given donor, are possible. As a result, the fit will recover an apparent distribution of distances even if the system is, in fact, rigid. This was confirmed in a separate series of simulations where we obtained a σ of 3.9 Å for f_l = 0.7, and a σ of 2.5 Å for f_l = 0.85. This apparent distribution effect must be taken into account in the analysis of real FRET data.

Table 5 shows also that the recovered value of the fraction of acceptor labeling f_l^c (fourth column) does not correspond to the value of f_l used to simulate the data set, but it is instead in good agreement with f_b. To understand this, we must consider that the parameter f_l^c is related to the fraction of donor fluorescence quenched by energy transfer to an acceptor. This fraction will be equal to the fraction f_l of acceptor labeling only if this is, in turn, equal to the probability of having an acceptor within a convenient transfer distance from the donor. This is no longer the case in a multi-acceptor. For example, for f_l = 0.8, using elementary statistics, we calculate that the probability of having at least one acceptor in one of the three closest F-actin subunits is 0.992. In other words, for the typical fraction of acceptor labeling of our samples (0.80–0.85), the recovered value f_l^c is still very close to unity. For such values of the fraction of acceptor labeling, f_l^c is expected to correspond to f_b when this is lower than unity, because only the fraction f_b of donor-labeled Tm bound to F-actin will be quenched by energy transfer. Therefore, in this particular case, f_l^c can be considered as the recovered value of the fraction of F-actin-bound Tm f_b^c.

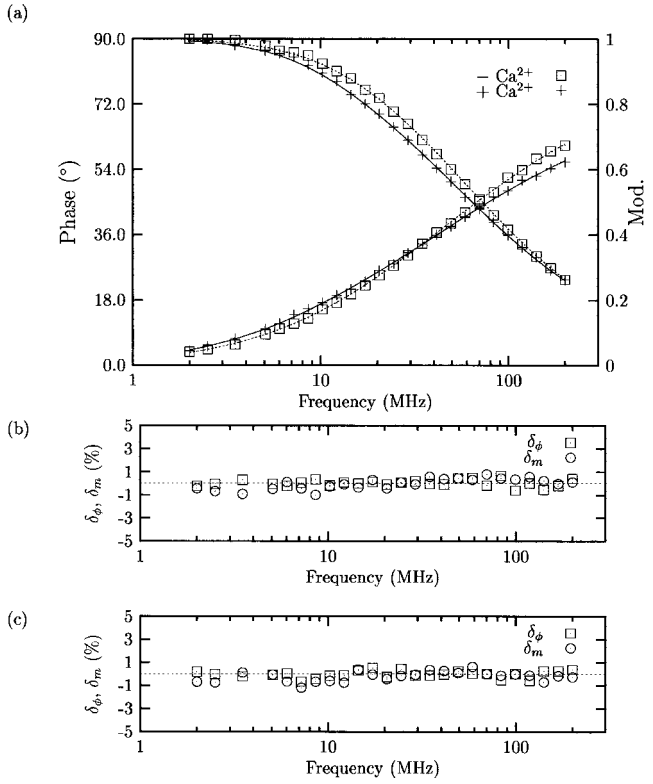

FIGURE 6 (*a*) Frequency-domain phase and modulation data in presence of energy transfer and fits for AEDANS donor- and TRITC-Ph acceptor-labeled F-actin·Tm·Tn complex in absence (□) and in presence (+) of Ca^{2+}. The fits were done using the distance distribution model (see text). The parameters recovered from the fits are reported in Table 6. (*b*) Phase (δ_ϕ) and modulation (δ_m) residuals of the fits in (*a*) for F-actin·Tm·Tn ($-Ca^{2+}$) and (*c*) for F-actin·Tm·Tn ($+Ca^{2+}$).

Distance distribution model fits of experimental data

Phase and modulation data for the AEDANS-TRITC-Ph D–A-labeled F-actin·Tm·Tn complex, in absence and in presence of Ca^{2+}, were fitted using the GAUDIS fitting function (double distance distribution), after successful testing for reliability against simulated data sets as described above. All fits were performed by fixing σ to the same value for both distances, optimizing the fraction f_1^c of acceptor labeling (which, as we have explained above, corresponds to the fraction of F-actin-bound Tm) and the two D–A distances r_1^c and r_2^c. The optimization was then repeated for a different value of σ until the best possible fit was achieved. The plot of the fits and of the corresponding residuals is shown in Fig. 6, the recovered parameters are reported in Table 6. The goodness of the fits was assessed by the χ_R^2 values and by the analysis of the residuals (see Fig. 6, *b* and *c*). All confidence intervals were calculated with the Support-Plane method (Johnson, 2000) at a probability of 95%.

The difference in the recovered distances r_1^c and r_2^c for the F-actin·Tm·Tn ($\pm Ca^{2+}$) complex (see Table 6, central columns) indicates a Tm movement due to [Ca^{2+}]. We also notice that the recovered apparent distances for the F-actin·Tm and the F-actin·Tm·Tn ($+Ca^{2+}$) complexes seem to be within ≈2–5 Å. This result would be in agreement with the assumption of a similar position for Tm in the two complexes, with a Tm radial distance that decreases by ≈2–3 Å in presence of Tn, as a result of a stronger interaction with F-actin of the Tm·Tn complex compared to Tm alone. A stronger Tm interaction in the presence of Tn is confirmed by an increased value of the fraction f_b^c of F-actin-bound Tm listed in the second column of Table 6 (the relation between recovered f_1^c and f_b^c has been discussed in the previous section) of 0.89 ± 0.01 (F-actin·Tm) and 0.98 ± 0.01 (F-actin·Tm·Tn ($\pm Ca^{2+}$)). The recovered width of the distance distribution σ (fifth column) is larger than an apparent distribution (see previous section) of 2.5 Å expected for a fraction f_1 of acceptor labeling of 0.85 in a rigid system. Therefore, we must assume a certain degree of flexibility in the F-actin·Tm·Tn complex, which can be due to flexibility of the proteins, to a distribution of azimuthal and axial orientations of Tm on F-actin, and to a slow component of the segmental motions of the labels. This last effect seems indeed to be important, because the width of the distance distribution σ appears to be only slightly affected by the presence of Tn, which may be expected to reduce considerably the Tm mobility in absence of Ca^{2+}.

TABLE 6 Double Gaussian distance distribution analysis of the D–A fluorescence decays

Sample	f_1^c (≡f_b^c)	r_1^c (Å)	r_2^c (Å)	σ (Å)	χ_R^2
F-actin·Tm	0.89 ± 0.01	25 ± 2	42.8 ± 0.8	7.7	1.1
F-actin·Tm·Tn ($-Ca^{2+}$)	0.98 ± 0.01	35 ± 1	40.4 ± 0.6	7.2	1.1
F-actin·Tm·Tn ($+Ca^{2+}$)	0.98 ± 0.01	23 ± 3	38.1 ± 0.6	7.7	1.4

Recovered parameters are: f_1^c, fraction of acceptor labeling (the equivalence $f_1^c \equiv f_b^c$ for this particular D–A system is discussed in the text); r_1^c, r_2^c, D–A distances; σ, width of the distance distribution.

DISCUSSION

Donor and acceptor positions

To locate the donor and the acceptor in the protein structures, the position of the labels were modeled as rigid segments attached to the sulfur atoms of the two Cys-190 of Tm, or to the β carbon of the hydroxyleucine of phalloidin on F-actin. The segment length corresponds to the distance between the sulfur atom linked to the label and the center of the aromatic system, which can be estimated from the label structure and is ≈9 Å for the AEDANS moiety on Tm and 10 Å for the TRITC moiety on phalloidin.

The location of the phalloidin binding site on F-actin was suggested first by EM data (Bremer et al., 1991) and proposed later by the atomic model of Lorenz (Lorenz et al., 1993). The latter result was subsequently confirmed by scanning transmission EM and three-dimensional helical

reconstruction (Steinmetz et al., 1998). The phalloidin site is at the junction of three actin subunits with the moiety interacting with subdomain four of one actin subunit, with subdomain three of the subsequent subunit located on the same strand, and with subdomain one of the subunit located on the other strand.

The segments representing the two donors on Tm are assumed to be oriented perpendicularly to the Tm axis, pointing outward, thus minimizing the interaction with the neighboring side chains of Tm chains. In this arrangement the AEDANS–AEDANS distance between the Tm chains, calculated from the Lorenz model (Lorenz et al., 1995), is ≈20 Å. We verified this assumption by measuring the distance between donor and acceptor labels across the chains at position 190. One Tm chain was donor-labeled with AEDANS and the other was acceptor-labeled with DABMI (R_0 = 39.9 Å) or *N*-(4-dimethylamino-3,5-dinitrophenyl)maleimide (DDPM) (R_0 = 27.2 Å) (Bacchiocchi and Lehrer, in preparation). The AEDANS–DABMI distance was found to be 18.1 ± 0.2 Å (σ = 1.0 ± 0.6 Å, χ^2_R = 1.3) using the CFS–LS (Johnson, 2000) global fitting program. Given the similar dimension of AEDANS and DABMI, this is in reasonable agreement with the expected result of 20 Å for the AEDANS–AEDANS distance and demonstrates that our model is essentially correct. The AEDANS–DDPM distance was found to be 15.5 ± 0.07 Å (σ = 1.4 ± 0.1 Å, χ^2_R = 1.7) in agreement with a DDPM length ≈3 Å shorter than DABMI.

We must point out that, for these relatively small separations, the distance resolution is far from optimum, due to the high value of R_0 compared to the measured distance r. In fact, the best resolution is reached when the ET efficiency is 50% ($r = R_0$). For the AEDANS–DABMI pair, in particular, the transfer efficiency is larger than 90%. To overcome this limitation, we also measured the longer distance between AEDANS at Cys-36 of gizzard β Tm and DABMI at Cys-56 of a gizzard αTm mutant in $\alpha\beta$Tm, where the α chain has a unique cysteine in position 56 (Bacchiocchi et al., in preparation). The D–A distance was found to be 33.2 ± 0.1 Å (σ = 4 ± 2 Å, χ^2_R = 1.1), again in good agreement with the approximate distance obtained from Lorenz model (Lorenz et al., 1995), which, taking into account the label dimensions, is ≈34 Å.

The acceptor position was modeled according to Heidecker et al. (1995) with a distance between two TRITC-Ph labels in adjacent F-actin subunits of 37.2 Å and a radial distance (from the F-actin axis) of 12.6 Å. The combined uncertainty in the donor and acceptor dimensions and positions is clearly difficult to estimate without a more direct way of locating them. However, given the reasonable assumptions of location, we believe that this uncertainty is likely to introduce an error not larger than a few angstroms in the measured D–A distances. In particular, this uncertainty will affect the absolute values of the distances in a similar way and it should cancel out when calculating the change of Tm position and orientation on F-actin.

Orientation factor, κ^2

In the calculation of R_0, for the various D–A pairs considered in this study, the orientation factor κ^2 (Eq. 16) was ⅔, the value averaged over a fast-reorienting and random distribution of label orientations. Discussions on the validity of this approximation, on the basis of substantial rapid reorientation of both donor and acceptor on the fluorescence time scale, have been presented: for Tm donor-labeled with AEDANS at Cys-190 (Tao et al., 1983), for F-actin acceptor-labeled with DABMI at Cys-374 (Tao, 1978), and for F-actin acceptor-labeled with TRITC-Ph (Heidecker et al., 1995). The good agreement between the modeled and the measured inter-chain distances on Tm, presented in the previous section, is a further confirmation of the correctness of this approximation.

MODELING OF Tm MOVEMENT

These data provide the first experimental evidence for the Ca^{2+}-induced movement of Tm on F-actin·Tm·Tn associated with the regulation of muscle contraction for a reconstituted thin filament system in solution. The difference in phase/modulation versus frequency data that Ca^{2+} produced was small but significant (Figs. 2 and 3). The data were fitted to two different models: an AC model coupled with a search algorithm that varies the position and orientation of Tm on F-actin, or by a DD model without any assumption as to the type of movement. Both models provided similar evidence for the type of Ca^{2+}-induced movement. Previous fluorescence studies did not obtain evidence for Tm movement. Our ability to detect movement was mainly due to improved resolution of both the frequency domain measurements and the data analysis. In particular, we used a more sensitive acceptor-labeling site on F-actin (phalloidin-binding site) and we quantitatively took into account several other parameters: the presence of two donors in different positions on Tm; the degree of acceptor labeling; the fraction of unbound Tm, and the multi-acceptor feature of F-actin.

Atomic coordinate model

The AC model used atomic coordinates of the F-actin·Tm structure with fixed positions of the two donors surrounded by six actin subunits containing acceptors as an initial basis for determining the best fit to the data during systematic changes in position and orientation of Tm on F-actin. The F-actin·Tm coordinates were obtained from the F-actin structure (Lorenz et al., 1993) and a model for the the coiled-coil Tm structure which has been refined by mini-

mizing the electrostatic energy between charged surface groups on Tm and F-actin (Lorenz et al., 1995). The Ca^{2+}-induced change in phase/modulation versus frequency data could be fit by moving Tm on F-actin azimuthally by ≈17° about the F-actin axis and ≈46° about its own inter-chain axis, with little change in radial position. The azimuthal change is in reasonable agreement with EM image reconstruction data, which suggest a movement of ≈20° (Xu et al., 1999). The new information, not available from EM data, is that Tm appears to rotate about its axis as well. Thus, Ca^{2+} causes Tm to roll over the F-actin surface. This is qualitatively reminiscent of the proposal of McLachlan and Stewart (1976), based on amino-acid sequence analyses of Tm. The large uncertainty in the angular changes may be related to a certain degree of flexibility of Tm on the surface of F-actin, and this seems to be reflected in the width of the distribution in the DD model (see below).

The Ca^{2+}-induced change in average transfer efficiency, calculated from our lifetime data, was close to zero for AEDANS at Cys-190 of Tm with both TRITC-Ph (see Table 3) and DABMI (data not shown) at different places on F-actin. Thus, in contrast to our lifetime measurements, steady-state measurements would not note a change in intensity, as previous measurements with the AEDANS and DABMI labels have shown (Miki et al., 1998). Calculation of the transfer efficiencies predicted by the model with changes in Tm position comparable to those observed in structural studies (Xu et al., 1999) showed very small changes (Table 2), in agreement with steady-state measurements. The analysis of our phase/modulation data could detect a change in the D–A distance due to effects on the distribution of lifetimes that can occur even without a net change in the total transfer efficiency. Clearly, accurate measurements of changes in lifetime contributions provide more information than average intensity measurements. In addition, the location of the TRITC acceptor probe at the phalloidin binding site gave larger changes than the DABMI acceptor at Cys-374, the place that the early lifetime study used (Tao et al., 1983).

Distance distribution model

To determine if a double DD model would be meaningful in this system, simulations were performed to obtain apparent distances modeling the changes in orientation of Tm on F-actin using information obtained from recent structural studies (Xu et al., 1999). The simulations used the distances from each of the donor labels on the two chains of Tm to acceptors on six of the closest subunits of F-actin, for three different positions of Tm on F-actin. For each position, four different combinations of initial values of fraction of labeled F-actin and degree of bound Tm were used. The two distances recovered agreed with the apparent distances, calculated from the geometry of the F-actin·Tm structure using Eq. 15, within 2 Å for all chosen initial values. This result demonstrates that a double Gaussian DD fitting procedure to the actual phase/modulation data is capable of recovering changes in apparent distance between the two donors on the Tm chains and the acceptors on the actin filament even in the presence of different degrees of acceptor labeling and unbound Tm.

The results for the real system (Table 6), showed an interesting difference in average apparent distance between labels. This difference was small for F-actin·Tm·Tn ($-Ca^{2+}$) (5 Å) and large for F-actin·Tm and for F-actin·Tm·Tn ($+Ca^{2+}$) (15–18 Å). It thus appears that the position of Tm is similar for F-actin·Tm and F-actin·Tm·Tn ($+Ca^{2+}$) but different for F-actin·Tm·Tn ($-Ca^{2+}$). Comparison with the distance differences obtained from the simulation (Table 5), indicates that the $-Ca^{2+}$ position corresponds to model *X* and the $+Ca^{2+}$ position to models *Y* or *Z* (Fig. 5). Thus, with this model, the addition of Ca^{2+} to F-actin·Tm·Tn appears to produce a movement of Tm either azimuthally or axially or both, although from the AC model it appears that both movements seem more likely. A similar rolling motion of Tm on the surface of F-actin has been observed in the S1-induced movement of smooth muscle Tm (Bacchiocchi et al., 2001). It should be noted that the recovered width of the distributions are very similar and are ≈5 Å greater than the value of 2.5 Å expected for a rigid system where Tm occupies a unique position on F-actin. Therefore, we must assume a certain degree of flexibility of the protein complex and the possibility that Tm participates in an equilibrium among two or more positions and that one of them is dominant depending upon $[Ca^{2+}]$. This second argument would be qualitatively in agreement with the three-state model of the F-actin·Tm·Tn thin filament proposed by McKillop and Geeves (1993), if we assume that the Ca^{2+}-induced shift of the blocked/closed/open equilibria from ~70%/25%/5% to ~0%/80%/20% can be correlated with corresponding equilibria between three different positions of Tm on F-actin.

Thus, solution evidence has now been obtained that strengthens the modified steric blocking models of regulation that are consistent with three Tm positions (McKillop and Geeves, 1993; Maytum et al., 1999; Lehman et al., 2000; Tobacman and Butters, 2000). It should be noted that, although our data only provide relative distances between sites on Tm and actin, we assume that the Ca^{2+}-induced movement involves only Tm, and we therefore cannot exclude small movements of actin.

We thank Dr. N. Golitsina and Ms. T. Freedman for help in the protein preparation, for the ATPase assays and for useful discussions.

This work was supported by National Institutes of Health (HL22461 and AR41637).

REFERENCES

Bacchiocchi, C., P. Graceffa, and S. S. Lehrer. 2001. Myosin-induced movement and actin-binding specificity of smooth muscle $\alpha\beta$ tropomyosin. *Biophys. J.* 80:357A. (abstract)

Bacchiocchi, C., and S. S. Lehrer. 2000. Multi-site fluorescence energy transfer shows Ca^{2+}-induced tropomyosin movement in reconstituted skeletal muscle thin filaments. *Biophys. J.* 78:364A. (abstract)

Bernstein, H. J. 1999. RasMol 2.7.1, Molecular Graphics Visualisation Tool—Based on RasMol 2.6 by R. Sayle. http://www.bernstein-plus-sons.com/software/rasmol/.

Bremer, A., R. C. Millonig, R. Sütterlin, A. Engel, T. D. Pollard, and U. Aebi. 1991. The structural basis for the intrinsic disorder of the actin filament: the "lateral slipping" model. *J. Cell Biol.* 115:689–703.

Cheung, H. C., C.-K. Wang, I. Gryczynski, W. Wiczk, G. Laczko, M. L. Johnson, and J. R. Lakowicz. 1991. Distance distributions and anisotropy decays of troponin C and its complex with troponin I. *Biochemistry.* 30:5238–5247.

Förster, T. 1948. Intermolecular energy transfer migration and fluorescence. *Ann. Phys.* 2:55–75.

Haselgrove, J. C. 1972. X-ray evidence for a conformational change in actin-containing filaments of vertebrate striated muscle. *Cold Spring Harbor Symp. Quant. Biol.* 37:341–352.

Heidecker, M., Y. Yan-Marriott, and G. Marriott. 1995. Proximity relationships and structural dynamics of the phalloidin binding site of actin filaments in solution and on single actin filaments on heavy meromyosin. *Biochemistry.* 34:11017–11025.

Huxley, H. E. 1972. Structural changes in actin- and myosin-containing filaments during contraction. *Cold Spring Harbor Symp. Quant. Biol.* 37:361–376.

Johnson, M. L. 2000. *CFS–LS* Global, Non-Linear, Least-Squares Fitting Program. Center For Fluorescence Spectroscopy, Baltimore, MD. http://cfs.umbi.umd.edu/cfs/software/.

Lakowicz, J. R. 1999. Principles of Fluorescence Spectroscopy, second Edition. Kluwer Academic/Plenum, New York.

Lakowicz, J. R., I. Gryczynski, and H. C. Cheung. 1988. Distance distributions in proteins recovered by using frequency-domain fluorometry. Applications to troponin I and its complex with troponin C. *Biochemistry.* 27:9149–9160.

Lakowicz, J. R., I. Gryczynski, W. Wiczk, J. Kusba, and M. L. Johnson. 1991. Correction for incomplete labeling in the measurement of distance distributions by frequency-domain fluorometry. *Anal. Biochem.* 195: 243–254.

Lakowicz, J. R., G. Laczko, H. Cherek, E. Gratton, and M. Limkeman. 1984. Analysis of fluorescence decay kinetics from variable-frequency phase shift and modulation data. *Biophys. J.* 46:463–477.

Lamkin, M., T. Tao, and S. S. Lehrer. 1983. Tropomyosin-troponin and tropomyosin-actin interactions: a fluorescence quenching study. *Biochemistry.* 22:3053–3058.

Lehman, W., R. Craig, and P. Vibert. 1994. Ca^{2+} induced tropomyosin movement in Limulus thin filaments revealed by three-dimensional reconstruction. *Nature.* 368:65–67.

Lehman, W., V. Hatch, V. Korman, M. Rosol, L. Thomas, R. Maytum, M. A. Geeves, J. E. Van Eyk, L. S. Tobacman, and R. Craig. 2000. Tropomyosin and actin isoforms modulate the localization of tropomyosin strands on actin filaments. *J. Mol. Biol.* 302:593–606.

Lehrer, S. S., and M. A. Geeves. 1998. The muscle thin filament as a classical cooperative/allosteric regulatory system. *J. Mol. Biol.* 277: 1081–1089.

Lorenz, M., K. J. V. Poole, D. Popp, G. Rosembaum, and K. C. Holmes. 1995. An atomic model of the unregulated thin filament obtained by x-ray fiber diffraction on oriented actin-tropomyosin gels. *J. Mol. Biol.* 246:108–119.

Lorenz, M., D. Popp, and K. C. Holmes. 1993. Refinement of the F-actin model against x-ray fiber diffraction data by the use of a directed mutation algorithm. *J. Mol. Biol.* 234:826–836.

Maytum, R., S. S. Lehrer, and M. A. Geeves. 1999. Cooperativity and switching within the three-state model of muscle regulation. *Biochemistry.* 38:1102–1110.

McKillop, D. F. A., and M. A. Geeves. 1993. Regulation of the interaction between actin and myosin subfragment 1: evidence for three states of the thin filament. *Biophys. J.* 65:693–701.

McLachlan, A. D., and M. Stewart. 1976. The 14-fold periodicity in α-tropomyosin and the interaction with actin. *J. Mol. Biol.* 103:271–298.

Miki, M., T. Miura, K.-I. Sano, H. Kimura, H. Kondo, H. Ishida, and Y. Maeda. 1998. Fluorescence resonance energy transfer between points on tropomyosin and actin in skeletal muscle thin filaments: does tropomyosin move? *J. Biochem.* 123:1104–1111.

Moré, J. J., B. S. Garbow, and K. E. Hillstrom. 1980. User guide for MINPACK-1. Argonne National Laboratory, Argonne, IL. http://www.netlib.org/minpack/.

Parry, D. A. D., and J. M. Squire. 1973. Structural role of tropomyosin in muscle regulation: analysis of the x-ray patterns from relaxed and contracting muscles. *J. Mol. Biol.* 75:33–55.

Rayment, I., H. M. Holden, M. Whittaker, C. B. Yohn, M. Lorenz, K. C. Holmes, and R. A. Milligan. 1993. Structure of the actin-myosin complex and its implications for muscle contraction. *Science.* 261:58–65.

Steinmetz, M. O., D. Stoffler, S. A. Muller, W. Jahn, B. Wolpensinger, K. N. Goldie, A. Engel, H. Faulstich, and U. Aebi. 1998. Evaluating atomic models of F-actin with an undecagold-tagged phalloidin derivative. *J. Mol. Biol.* 276:1–6.

Straume, M., and M. L. Johnson. 1992. Monte Carlo method for determining complete confidence probability distributions of estimated model parameters. *In* Numerical Computer Methods. L. Brand and M. L. Johnson, editors. Vol. 210 of Methods in Enzymology. Academic Press, Inc., San Diego. 117–129.

Tao, T. 1978. Nanosecond fluorescence depolarization studies on actin labeled with 1,5-IAEDANS and dansyl chloride. Evidence for label flexibility. *FEBS Lett.* 93:146–150.

Tao, T., M. Lamkin, and S. S. Lehrer. 1983. Excitation energy transfer studies of the proximity between tropomyosin and actin in reconstituted skeletal muscle thin filaments. *Biochemistry.* 22:3059–3066.

Tobacman, L. S., and C. A. Butters. 2000. A new model of cooperative myosin-thin filament binding. *J. Biol. Chem.* 275:27587–27593.

Van Der Meer, B. W., G. Coker, III, and S.-Y. S. Chen. 1991. Resonance Energy Transfer, Theory and Data. Wiley-VCH, New York.

Waggoner, A., R. DeBiasio, P. Conrad, G. R. Bright, L. Ernst, K. Ryan, M. Nederlof, and D. L. Taylor. 1989. Multiple spectral parameter imaging. *Methods Cell Biol.* 30:449–478.

Xu, C., R. Craig, L. Tobacman, R. Horowitz, and W. Lehman. 1999. Tropomyosin positions in regulated thin filaments revealed by cryoelectron microscopy. *Biophys. J.* 77:985–992.